coatings

MDPI

Review

Surface Enhanced Raman Scattering Substrates Made by Oblique Angle Deposition: Methods and Applications

Hin On Chu, Shigeng Song *, Cheng Li and Des Gibson

SUPA (Scottish Universities Physics Alliance), Institute of Thin Films, Sensors and Imaging, School of Engineering and Computing, University of the West of Scotland, PA1 2BE Paisley, Scotland, UK; Hinon.Chu@uws.ac.uk (H.O.C.); Cheng.Li@uws.ac.uk (C.L.); Des.Gibson@uws.ac.uk (D.G.)

* Correspondence: Shigeng.Song@uws.ac.uk; Tel.: +44-141-848-3630

Academic Editor: Alessandro Lavacchi

Received: 29 December 2016; Accepted: 6 February 2017; Published: 15 February 2017

Abstract: Surface Enhanced Raman Spectroscopy presents a rapid, non-destructive method to identify chemical and biological samples with up to single molecule sensitivity. Since its discovery in 1974, the technique has become an intense field of interdisciplinary research, typically generating >2000 publications per year since 2011. The technique relies on the localised surface plasmon resonance phenomenon, where incident light can couple with plasmons at the interface that result in the generation of an intense electric field. This field can propagate from the surface from the metal-dielectric interface, so molecules within proximity will experience more intense Raman scattering. Localised surface plasmon resonance wavelength is determined by a number of factors, such as size, geometry and material. Due to the requirements of the surface optical response, Ag and Au are typical metals used for surface enhanced Raman applications. These metals then need to have nano features that improve the localised surface plasmon resonance, several variants of these substrates exist; surfaces can range from nanoparticles in a suspension, electrochemically roughened electrodes to metal nanostructures on a substrate. The latter will be the focus of this review, particularly reviewing substrates made by oblique angle deposition. Oblique angle deposition is the technique of growing thin films so that the material flux is not normal to the surface. Films grown in this fashion will possess nanostructures, due to the atomic self-shadowing effect, that are dependent mainly on the deposition angle. Recent developments, applications and highlights of surface enhanced Raman scattering substrates made by oblique angle deposition will be reviewed.

Keywords: surface enhanced Raman spectroscopy; coatings on polymer; special substrate materials; metal coatings; deposition, characterisations and applications of sculptured and textured thin films

1. Introduction

Raman scattering is the inelastic scattering of light, first discovered in 1928 [1], from molecular vibrations. It was found that in Raman scattering, the energy shift of the scattered photon is either higher in energy than the incident photon (anti-Stokes shift) or lower energy (Stokes shift). The shift will be unique to the type of molecular vibrations, therefore, spectral 'fingerprints' can be used to identify samples. For example, Raman spectroscopy can be used to identify the differences between natural and synthetic diamonds [2]. Not only is Raman spectroscopy a powerful technique for identification of samples, but it also requires little to no sample preparation, non-destructive and complementary with other techniques such as infrared spectroscopy. One major weakness of this technique is that Raman scattering is a naturally weak effect. Therefore concentrated samples or long measurement times are required to obtain reasonable spectra. Advanced Raman techniques such as surface enhanced Raman spectroscopy or scattering (SERS) are capable of getting around this issue.

1.1. Surface-Enhanced Raman Scattering

The SERS phenomena was first reported in 1974 [3], where abnormally high Raman signal was observed for pyridine adsorbed onto an electrochemically roughened silver electrode. Since then, there have been competing theories into what exactly the enhancement mechanism is, but two types of mechanisms have been proposed. One being a chemical mechanism [4], here the molecule is chemisorbed to the surface and the incident light is able to excite an electron from the highest occupied molecular orbital (HOMO) into an unoccupied molecular orbital through indirect coupling with the metal. This is also known as the charge transfer mechanism. Alternatively, the laser may be in resonant with the molecule-metal complex and can directly excite an electron from the HOMO directly into an unoccupied orbital. Figure 1 demonstrates the basic schematic of this.

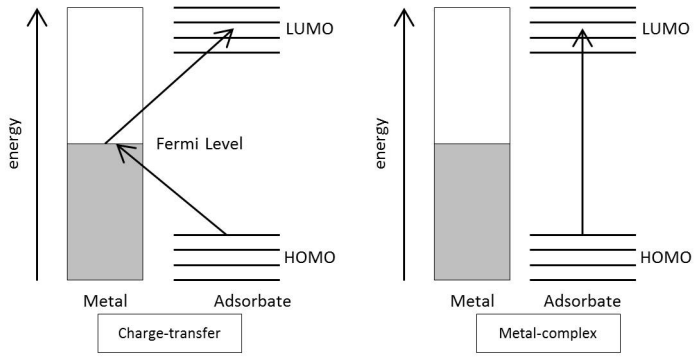

Figure 1. Schematic of common chemical mechanisms for SERS enhancement. The charge transfer involves the indirect excitation through the metal. In the metal-adsorbate complex, the incident photon can be resonant with the electronic transition between the highest occupied molecular orbtial (HOMO) towards the lowest unoccupied molecular orbital (LUMO).

The exact chemical mechanism is still debated, such as by Chen et al. [5], who found that the chemical enhancement, based on their calculations, is largely based on the metal cluster charge. Anionic clusters were found to relatively occupy higher energies, in the metal-pyridine complex, as well as having more delocalized electrons. This meant an increase in the polarizability thus leading to the non-resonant Raman enhancement. An issue with the chemical enhancement mechanism is that is can only account for short-range interactions as well as relatively low enhancements. Chemical enhancement cannot accurately describe the high SERS enhancement factors (EF) that has been reported, some as high as 10^{14} [6], particularly when single-molecule sensitivity is involved. Initial arguments for the SERS enhancement involved an increase in surface area, however, this alone could not account for the many orders of magnitude enhancement of the Raman cross section. Another SERS enhancement mechanism that was the proposed was the electromagnetic mechanism (EM). In 1977, Jeanmaire and Duyne had reported a systematic experiment to determine the mechanism of SERS enhancement [7]. This review will go into more detail regarding the electromagnetic mechanism in Section 2, but to simplify; the EM can approximate the single-molecule SERS enhancement factor (a measure of how much the Raman signal is increased compared to the non-SERS condition) as given in Equation (1). This is applicable when the laser frequency (ω_L) $\approx$ the radiated frequency (ω_R).

$$EF = \frac{|E_{LOC}(\omega_L)|^2 |E_{LOC}(\omega_R)|^2}{|E_{INC}|} \approx |E_{LOC}|^4 \quad (1)$$

This approximation, while not applicable to all circumstances, provides an estimate of the SERS EF that can be derived from the localised electric field (E_{LOC}). E_{INC} is the incident electric field. Typically, experimentally derived EF, known as the analytical SERS EF, can be calculated from Equation (2). I_{SERS}

and I_{BULK} is the Raman intensity for the SERS and bulk Raman measurement respectively, N_{SERS} and N_{BULK} is the number of molecules involved in the SERS and bulk Raman measurement respectively.

$$EF = \frac{(I_{SERS}/N_{SERS})}{(I_{BULK}/N_{BULK})} \quad (2)$$

The number of molecules involved with the Raman measurements is often difficult to determine with accuracy. Calculations must be careful, errors with the reference have led to reports of EF as high as 10^{14} [8]. In [8] the Raman cross-section of crystal violet (CV) was compared to non-SERS cross-section of methanol. CV and methanol have significantly different non-SERS Raman cross-sections, methanol's non-SERS Raman cross-section is approximately 5×10^6 smaller than crystal violet's, so the reported EF would be likely have overestimated by a factor of 10^6. A comprehensive study on SERS enhancement factors identifies this and states that the SERS EF only needs to be 10^7 for single-molecule sensitivity [9]. In the electromagnetic mechanism, a SERS surface uses the localised surface plasmon resonance (LSPR) phenomenon, where an incident photon excites a conduction band electron of a structure smaller than the incident photon wavelength. These plasmons oscillate locally and its frequency is known as the LSPR, this propagates an electric field and any molecule that is close enough proximity will experience an enhanced Raman efficiency. LSPR depends on a number of factors, such as material, size and geometry of the surface. It is also found that when nanoparticles are within close proximity, their electric fields can couple to produce an intense region of enhanced Raman scattering. These are sometimes called 'hotspots', and are a goal in SERS research to be able to fabricate as many hotspots on a substrate. There have been numerous studies into the effects of size, shape and material on LSPR [10,11], however, covering these studies is outside the scope of this review. In order to fabricate nanostructures with large LSPR, several approaches to SERS surfaces include: colloidal nanoparticles [12,13], roughened electrodes [3,14] and nanostructures on a substrate (such as glass [15,16] or polymers [17–19]). This review will explore latter type of SERS substrates, particularly those made by oblique angle deposition (OAD).

1.2. Introduction to Oblique Angle Deposition

The definition of oblique angle deposition is not consistent, and is sometimes called glancing angle deposition (GLAD), in general the term is meant for depositions that use material fluxes angled away from the substrate normal. GLAD is an extension of OAD, the term is used to indicate substrate motion and high deposition angles (i.e., >80°). OAD had been a focus of scientific research since the 90s [20–22], from multi-component nanostructures to spiral photonic crystals, today it is still a valuable technique for producing controlled nanostructured films for a wide range of applications [23–26]. The growth mechanism differs from growing metal films at normal, where after the formation of nanoclusters at nucleation sites, a continuous film is gradually formed [27]. In OAD, nanostructuring of the thin film begins when material deposited onto the surface start shadowing incoming material, this is known as the atomic self-shadowing effect [28]. If adatom surface diffusion is limited only to along the nanorod, then the cosine rule (see Section 3.1) could potentially be used to model OAD nanostructure angles [29]. Physical vapour deposition (PVD) techniques have applied OAD for making nanostructured thin films, from electron beam deposition [30] to DC sputtering [31], OAD is a popular PVD method for making SERS substrates. Figure 2 shows two different PVD approaches, specifically in these images are DC magnetron sputtering and electron beam deposition. In sputtering deposition, a target is bombarded by high energy particles that eject material. Different set-ups are used, in Figure 2a(top) a rotating drum configuration is selected, whereas in the bottom we see an oblique angle deposition set-up where the substrate is mounted on angled wedges. Sputtering techniques are rare for OAD type SERS substrates, because these set-ups use a planar source so the lack of material flux collimation will affect the self-atomic shadowing effect. Figure 2b is an example of an electron-beam deposition system with planetary rotation. In this type of PVD, a beam of electrons is focused onto a material source under high vacuum. To ensure collimation, OAD set-ups are done so that the distance between substrate

and source is far greater than the diameter of the evaporation source. An advantage of electron-beam deposition is that source sizes can be varied more easily than in magnetron sputtering, as one electron gun can have different source holders, whereas the sputter target size is dictated by magnetron size.

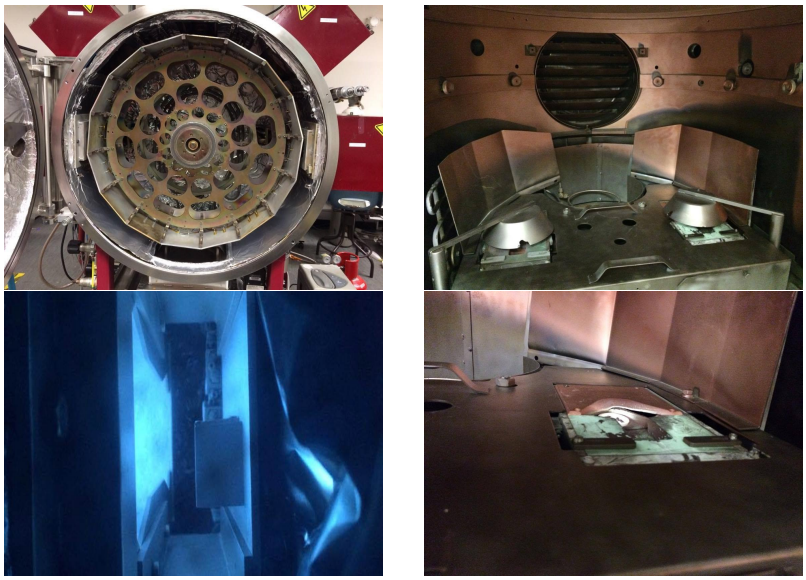

(**a**) DC magnetron sputtering (**b**) e-beam deposition

Figure 2. (**a**) DC magnetron sputtering system, typical configuration (**top**) involves a rotating drum so co-sputtering is available. (**bottom**) Substrates could be mounted onto a wedge in front of the target for OAD; (**b**) (**top**) An electron-beam deposition system, in this set-up two sources are available for co-depositions (**bottom**) an example of an e-beam gun, electrons are ejected from a tungsten filament and directed by both a permanent and electromagnet.

The general scheme for an oblique angle deposition is given in Figure 3. As mentioned before, in OAD the substrate is tilted from the material flux and from the atomic self-shadowing effect nanostructures appear in the thin films. Here α is the deposition angle, β is the resultant nanostructure angle.

More discussion and detail into OAD will be given in Section 3, in brief OAD presents a simple method for fabricating complex nanostructured thin films, utilizing this and knowledge of LSPR in nanostructures, high performance SERS substrate fabrication is realised. This review will explore simulation techniques to understand SERS substrates, OAD approaches towards SERS substrate fabrication and finally their applications.

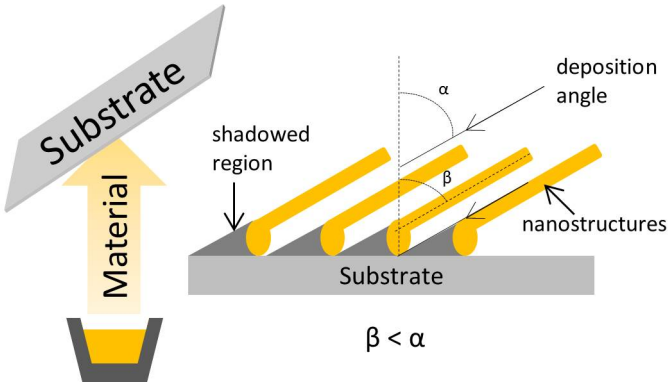

Figure 3. Scheme of oblique angle deposition and how the resultant angle β is influenced by the atomic self-shadowing effect, that is affected by surface structures and the deposition angle, α.

2. Simulations of the SERS Effect

This section will briefly outline approaches to simulating SERS substrates, particularly the computational electrodynamics for enhancement factor derivations. Computational electrodynamics has become an integral part of understanding the SERS enhancement, as previously discussed, the SERS enhancement is appoximately the fourth power of the localised electric field (1). Therefore knowledge of the local electric fields at the nanostructured surfaces is important to derive an approximation of the SERS EF. For example, shape of nanostructures for SERS can lead to significantly different enhancement factors. Rodrigues et al. have published a study into the use of different nanostructured SERS substrates [32]. In this study, the enhancement factors of roughened electrodes, Au fixed nanotubes, Klarite® (was a commercially available SERS substrate based on Si substrates that have been treated with nanolithography) and a nanosphere suspension is summarised in Table 1.

Table 1. Comparison of different SERS substrate enhancement factors. In [32] the Raman probe is 10^{-2} M 4-mercaptopyridine, based on the vibrational band at 1090 cm^{-1} (for the nanosphere suspension the EF is based on the 1000 cm^{-1} band). 1,2-Bis(4-Pyridyl)Ethylene was used for dimer-on-mirror substrates, thionine acetate was used on gold-coated nanorod array, data extracted from [32–34].

SERS Substrate	Enhancement Factor	Reference
Roughened electrode	$39.0 \pm 73.0 \times 10^3$	[32]
Gold fixed on 400 nm diameter nanotubes	$120.0 \pm 50.0 \times 10^3$	[32]
Klarite®	$4.2 \pm 2.0 \times 10^3$	[32]
Nanosphere suspension	$1.4 \pm 0.14 \times 10^3$	[32]
Dimer-on-mirror substrate	1.2×10^{11}	[33]
Gold-coated Nanorod Array	$\sim 10^7$	[34]

As indicated in Table 1, the shape, size and order of nanostructures can give orders of magnitude difference in SERS performance. Colloidal nanoparticles suspensions were one of the earliest SERS systems to demonstrate high sensitvity [8], however, these SERS surfaces depend on nanoparticle separation which determines the generation of hotspots. Other types of SERS substrates have been reported to produce enhancement factors of up to 10^{11} [33]. The EF for Klarite® also seems rather low considering this type of SERS substrate is capable of producing EFs in the range of 10^6 [35], Rodrigues et al. attribute this low enhancement to the fact that there is no strong hot spots in the SERS mapped area which leads to lower enhancements being measured. In order to better understand how to obtain SERS performance, it is a good start to understand the local electric fields of a surface; computational electrodynamics is often utilised to understand this.

2.1. Computational Electrodynamics

Advances in high performance computing have meant more computationally expensive simulations become available. Computational methods to derive the electric fields and optical responses have led to popular methods such as: finite-element method (FEM) [36], Mie theory [32], finite difference time domain (FDTD) [37] and discrete dipole approximation (DDA) [17,38]. In oblique angle depositions, nanostructures are typically aspherical, as Mie theory describe the light scattering from spherical particles, approaches to derive the electric fields for arbitrary geometries will be considered for this review. Therefore the methods FDTD and DDA will be considered, while finite element methods have been used in SERS studies, there is little in literature regarding OAD derived SERS substrate studies using FEM.

2.1.1. Finite Difference Time Domain

One way of deriving the electric field is the finite difference time domain method. Finite differences are used as approximations for the spatial and temporal derivatives in Maxwell's equations.

The starting point for most FDTD sovlers begin with the time-derivative components of Maxwell's Equations (3) and (4).

$$\frac{\delta \mathbf{B}}{\delta t} = -\nabla \times \mathbf{E} - J_B \tag{3}$$

$$\frac{\delta \mathbf{D}}{\delta t} = +\nabla \times \mathbf{H} - \mathbf{J} \tag{4}$$

E and **H** are the macroscopic electric and magnetic fields. **J** and $\mathbf{J}_B$ are the electric-charge and magnetic-charge current density respectively. **B** and **D** are the magnetic induction and electric displacement fields [39]. Time-domain calculations initiate where fields and currents are zero. Temporal and spatial components would then be discretised into a grid, where a Cartesian volume can be used for spatial discretisation. The Yee scheme is commonly used for spatial discretisation [40–42] and time steps are used for the temporal discretisation. Oskooi et al.'s interactions with other photonics researchers found that FDTD codes were developed to address their needs, this would be time consuming and so open-source packages such as MEEP (MIT Electromagnetic Equation Propagation) enable easier access to FDTD calculations [40]. FDTD studies are typically done to find the electric fields around the nanostructures in order to understand the SERS EF from an EM perspective [43,44]. A notable application of 3D-FDTD for understanding SERS enhancements was in a study by Liu et al. [44].

It is difficult to experimentally determine the electric field for nanostructures, however, in [44] FDTD was used to evaluate the electric field distribution based on s and p polarised light (see Figure 4). It was found that the electric field was more intense towards the base of the Ag film, paricuarly for s polarised light. The article mentioned that it would be interesting to know whether these results could actually contribute to the SERS enhancement, since these hot spots were under the nanorods. To investigate this further, they deposited trans-1,2-(4-pyridyl)ethene (BPE) onto smooth silver film and then used OAD to fabricate nanorods over this layer. SERS measurements were compared before and after this, as simulation results showed more indense electric fields towards the bottom of the Ag film, so initially it is thought that the SERS intensities for BPE just at the bottom of the nanorods would be comparable with the case where there is full coverage. This was found to not be the case, the results showed that the sides and top of the nanorods contributed greater than the hotspots towards bottom of the rods. It was also observed that the s polarised light gave greater Raman intensities, a result that was consistent with the FDTD calculations. FDTD has also been used to investigate the anisotropic effects of using different objectives and apatures for SERS measurements [45]. Here, the linear relationship of larger apature with Raman intensity was observed to breakdown for large (solid angle > 1) numerical apatures. Raman scattering is an anisotropic effect, therefore it would be logical at increasing the numerical apature may not linearly increase the observed Raman intensities. By converting a captured image of the nanostructures made by OAD, then using 6 levels of grey to assign the Ag step height, a 3D representation was obtained for FDTD simulations. Figure 5 illustrates their FDTD results for two different film thicknesses of Ag.

In their 60 nm film, effects from larger numerical apatures are less pronounced and is interpreted as the taller nanorods enable dipole resonances in more directions than their thinner metal film. The 30 nm film is suggested to confine dipole resonances in the xy plane, this is supported by the significantly smaller change in $|E|^2_{MAX}$ for the film with taller nanorods. These outputs have shown how valuable FDTD is for understanding SERS enhancements, however, FDTD is effective for refractive indices ≥ 1.4 [46]. Computationally these are still expensive, especially when simulating large 3D arrays. Next the discrete dipole approximation will be reviewed for its applications to OAD derived SERS substrates.

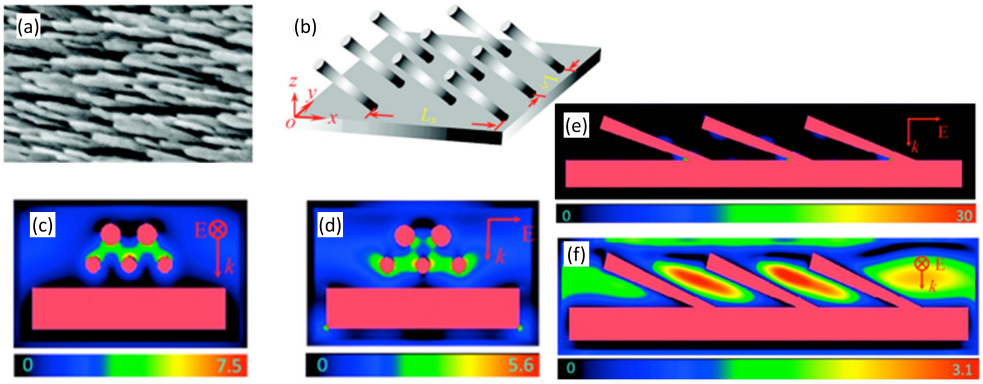

Figure 4. Modelling of input (**b**) based on nanorods as seen in the SEM image (**a**). 3D-FDTD simulation of the electric field distribution, the electric field distribution calculated for λ = 785 nm. Results show that the electric field distribution for p-polarised in the xz and yz (**c**,**e**) and s-polarised light in the same planes (**d**,**f**). Reprinted with permission from [44]. Copyright 2009 American Chemical Society.

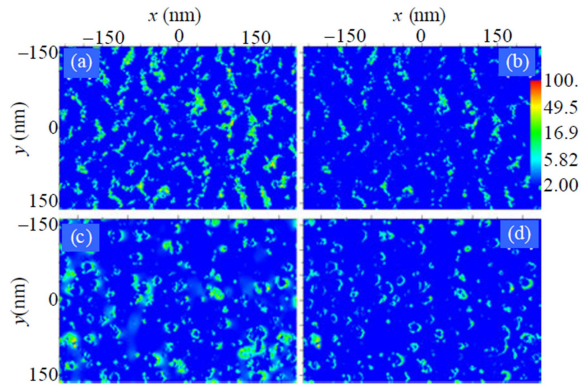

Figure 5. Cross-section logarithmic plots of the field enhancement $|E|^2$ at 514 nm excitation. (**a**,**b**) are the base of the 30 nm Ag nanoislands at NA = 0.12 ($|E|^2_{MAX}$ = 85) and 0.85 ($|E|^2_{MAX}$ = 50) respectively. (**c**,**d**) are cross-sections at the tip of the 60 nm nanoislands, NA = 0.12 ($|E|^2_{MAX}$ = 70) and 0.85 ($|E|^2_{MAX}$ = 67) respectively. Reprinted with permission from [45]. Copyright 2012 by Jayawardhana et al; article under the terms of the Creative Commons Attribution License.

2.1.2. Discrete Dipole Approximation

Discrete dipole approximation is another computational method for calculating light scattering and absorption for arbitrary geometries. DDA approximates the target geometry into an array of polarisable points, each point is defined as a dipole, where each dipole interacts with each other through their electric field. This approach is applicable where particles are comparable in size to the wavelength (λ) and can be used for inhomogenous targets. DDA can provide near-field evaluations, using the polarisations the electric (see Equation (5)) and magnetic fields can be derived for any point in 2D periodic targets [47].

$$\begin{aligned}\mathbf{E}(\mathbf{r},t) =& e^{-i\omega t}\sum_j \sum_{m,n}{}' \frac{exp(ik_0 R_{jmn})}{|R_{jmn}|^3}\phi(R_{jmn})\{k_0^2\mathbf{R}_{jmn}\times(\mathbf{P}_{jmn}\times\mathbf{R}_{jmn}) \\ &+ \frac{(1-ik_0\mathbf{R}_{jmn})}{\mathbf{R}_{jmn}^2}[3\mathbf{R}_{jmn}(\mathbf{R}_{jmn}\cdot\mathbf{P}_{jmn}) - \mathbf{R}_{jmn}^2\mathbf{P}_{jmn}]\} \\ &+ \mathbf{E}_0 exp(i\mathbf{k}_0\cdot\mathbf{r}-\omega t)\end{aligned} \quad (5)$$

The $\phi(\mathbf{R}_{jmn})$ function suppresses oscillating contributions from distant dipoles, so that summations can be truncated and is defined in (6):

$$\phi(\mathbf{R}_{rmn}) \equiv exp[-\gamma(k_0 R)^4] \times \begin{cases} 1 & for\ R \geq d \\ (R/d)^4 & for\ R < d \end{cases} \quad (6)$$

$\mathbf{P}_{jmn}$ is the polarisation, $\mathbf{R}_{jmn}$ is defined as $\mathbf{r} - \mathbf{r}_{jmn}$, the location of (m,n) replica of dipole j ($\mathbf{r}_{jmn}$) is related as $\mathbf{r}_{j00}$ + m$\mathbf{L}_u$ + n$\mathbf{L}_v$. $\mathbf{L}_u$ and $\mathbf{L}_v$ are lattice vectors for the DDA array. The most computationally intensive components of either the electric or magnetic field calculations is the summations, despite large memory requirements, accurate DDA calculations can be performed on modern desktops with number of dipoles on the order of 10^6. There are several open source DDA codes available, however it is the DDSCAT code that is particularly noted for use with periodic targets. Oblique angle deposition for SERS substrates typically generates randomly distributed arrays of nanostructures [30], and it was found in a recent study by Wei et al. that the random distribution of nanorods would generate greater SERS enhancements than regular arrays [38]. Figure 6 shows the adapted results from the study in [38], different shapes of nanostructures were used for this study, a comparison was made between individual and 2D arrays.

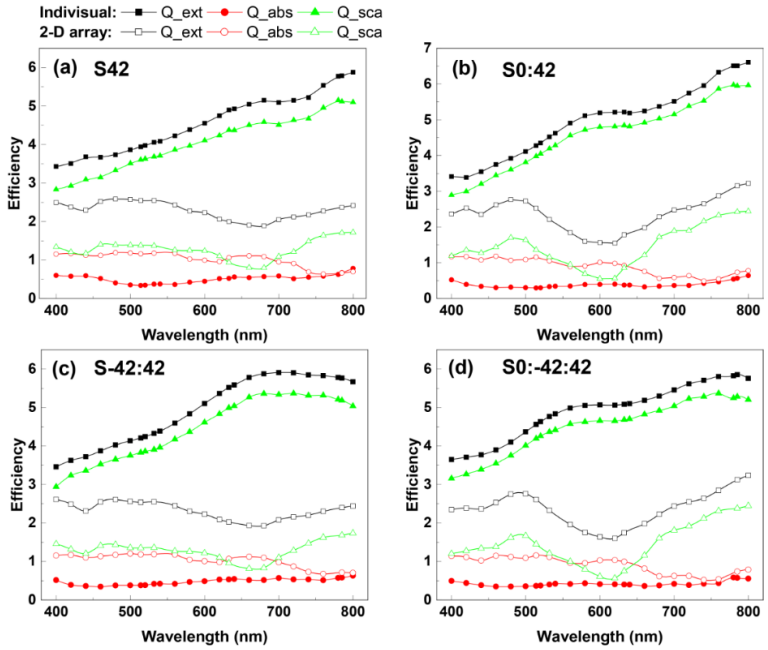

Figure 6. The extinction, scattering and absorption efficiencies are calculated for different nanorod shapes: (**a**) S42; (**b**) S0:42; (**c**) S-42:42; (**d**) S0:-42:42. Here we see that the calculated EFs are consistently higher than their 2D array analogues. These optical properties correlate with the coupling with neighbouring nanorods in the array. Reprinted with permission from [38]. Copyright 2015 by Wei et al; licensee Beilstein-Institut., article under the terms of the Creative Commons Attribution 2.0 License.

Figure 7 defines the DDA target shapes and dimensions used by Wei et al. Despite the higher scattering efficiencies for individual nanostructures, a good SERS substrate should have as much measurement consistency, where a random array will inevitably produce variations across the surface.

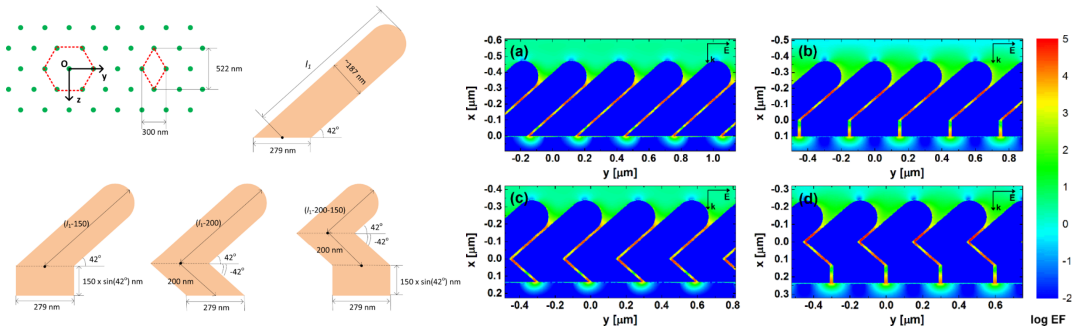

Figure 7. (**left**) The definition of the nanorod shapes and periodicity used in this DDA study. (**right**) DDA results showing the EF logarithmically, the shapes are defined as (**a**) is unit target S42, (**b**) S0:42, (**c**) S-42:42, (**d**) S0:-42:42. Reprinted with permission from [38]. Copyright 2015 by Wei et al; licensee Beilstein-Institut., article under the terms of the Creative Commons Attribution 2.0 License.

This study also investigated the anisotropic nature of SERS EF, as the EF has an asymmetric angular dependence of the excitation incident angle. These observations was compared to an earlier study by Liu et al. [48] and were interpreted with a modified Greenler's model where the molecule is treated as a dipole on the nanorod length. This model explains the asymmetry in SERS EF for nanorod arrays, as different polarisations can excite the dipoles depending on the molecular-surface arrangement. Another application of DDA for understanding OAD derived SERS substrates was done in the study by Keating et al. [17]. Here different nanostructures were obtained by using a nano-imprinted polymer template for oblique angle deposition. Nanorods with supports were investigated, where the SERS EF from the EM mechanism was studied using DDA. The models used here were adapted and used by Wei et al.'s paper so are similar to the schematic in Figure 7. In this earlier work, DDA was used to calculate the SERS enhancements for Cu and Ag nanorods. The simulations were consistent with experimental observations, where the enhancements for Cu based nanorods were smaller than their Ag analogues. Like FDTD, DDA has its advantages with the computations for arbitrary geometries, where DDA accuracy is determined by the inter-dipole spacings.

3. Oblique Angle Deposition Methods

As discussed in the previous section, nanoparticle shape and separation effectively determine SERS performance. Oblique angle deposition is a powerful technique, reported use of OAD go further than a hundred years ago [49]. Since then, OAD has expanded into a vast range of applications; biosensing [50], broadband anti-reflection coatings [51] and optical Rugate filters [52]. Figure 8 demonstrates a range of structures that can be achieved through OAD.

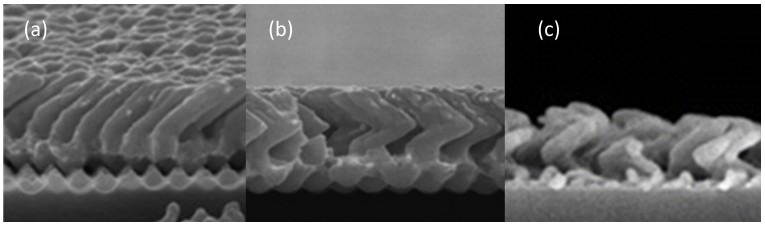

Figure 8. Examples of nanostructures that can achieved through oblique angle deposition. (**a**) Nanorods (**b**) Nanochevons, sometimes called zig-zag nanocolumns (**c**) Helical nanocolumns can be achieved through substrate rotation during deposition. Reprinted with permission from [17,53]. Copyright 2014 American Chemical Society.

Films made by OAD will differ from those made by normal-depositions. As discussed in the paper by Zhao et al. [28], this technique applies the atomic self-shadowing effect which will produce

porous thin films. Unlike normal-deposited thin films, the material's properties can affect the resultant film, such as surface-diffusion will occur easier for metals than other optical materials (i.e., oxides). Oblique angle deposition for SERS substrates can be characterised into two main categories; pure metal SERS substrates and metal-decorated OAD-derived nanostructures. These are the common routes into making SERS scattering substrates and this section will review the range of techniques involved.

3.1. Metal Nanostructures for SERS

Noble metals such as gold, silver and copper are typically used as SERS materials because of their optical properties in the visible region. OAD provides a route to producing nanostructured thin films for SERS applications, electron-beam evaporation is typically used for OAD configurations. However, other OAD set-ups have been used with sputtering depositions [54]. Sputter deposition is more typical for depositing nanoparticles onto a surface, which will be covered in the next section, and is not as popular a choice as sputtering set-ups use planar sources so atomic self-shadowing effects will need to be reconsidered. In planar targets, material flux can come from a wider range of angles, thus affecting how atomic self-shadowing will occur at the surface. Two popular relations for describing the tilt of nanostructures in OAD are the tangent rule (7) [55] and the cosine rule (8) [29], where the cosine rule is more applicable for higher deposition angles ($\alpha > 60^\circ$).

$$\tan\alpha = 2\tan\beta \tag{7}$$

$$\beta = \alpha - \arcsin\left(\frac{1-\cos\alpha}{2}\right) \tag{8}$$

These relations do not describe metal systems very well, materials such as silver tend to get nanorod angles of approximately 70°–75° when deposited at 86° [56]. These rules are geometric arguments for predicting the resultant angles from OAD, so there must lie other processes that affect the β angle. Alternative approaches have been investigated [57,58], there are so many empirical relations made for OAD but the more accurate predictions are material dependent. For example, one modification to Equation (8) was realised in [18] as a simple coefficient in front of the arcsin term, however this only works well for high α and Ag.

$$\begin{aligned} &\beta = \alpha - \chi\arcsin\left(\frac{1-\cos\alpha}{2}\right) \\ &\chi \approx 0.588 \end{aligned} \tag{9}$$

As Equations (7) and (8) are geometrically derived, where Equation (8) only takes surface diffusion into account along a nanorod [29], thermally activated effects are not taken into account. Temperature studies for oblique angle depositions have been conducted, into how substrate temperature affects the resultant nanostructures.

3.1.1. Temperature Dependent Oblique Angle Deposition

The effect of substrate temperature has been a topic of interest for SERS researchers, particularly those using the oblique angle deposition configurations [16,43,59]. Compared to other materials typically used in OAD, silver and gold tend to have significantly lower surface diffusion activation energies, this means adatoms can more readily take part in thermally activated effects. Khare et al. had found that for elevated substrate temperatures, at 573 and 623 K, temperature induced adatom surface diffusion can negate the atomic self shadowing effect for Ag films [60]. Normally a substrate would become hotter during depositions, one way to control this is to fit a substrate temperature controller into the set-up. A study by Singh et al. demonstrated a SERS substrate consisting of Ag nanorods grown at 140 K required lower deposition times to get the same nanorod lengths as those done at room temperature [59]. Not only this, they had found that it also showed greater sensitivity than

the substrate made at room temperature. Figure 9 illustrates the difference in SERS intensity when comparing the substrate made at room temperature and at 140 K.

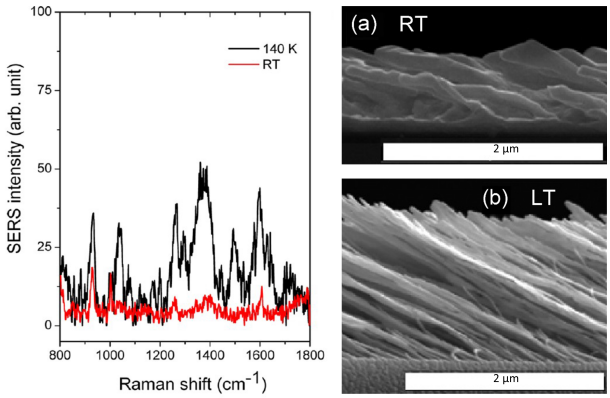

Figure 9. SERS spectra for BPE on two SERS substrates made by OAD at two different substrate temperatures. SEM images for the substrates deposited at (**a**) room temperature (**b**) 140 K. Reprinted with permission from [59]. Copyright 2012 American Chemical Society.

The difference in relative peak intensities at 1610 and 1640 cm^{-1} indicates different molecular interactions at the surface. As these Raman shifts are representative of the aromatic ring stretching mode and in-plane ring mode, the molecular orientation to the surface must be different for each substrate. Another point to note in this study, is that while the substrate is kept at 140 K with a liquid nitrogen cooling block during deposition. It is worth noting that because the substrate is at lowered temperatures in the vacuum chamber, it would be possible for it to act as a Meissner trap thereby attracting unwanted impurities onto the substrate. This may explain why there are some smaller bands found in the spectra, that the authors have attributed to organics from the environment or outgassing from the vacuum system. Coupled with their FDTD calculations, it was found that the pores formed from deposition at 140 K to generate hotspots for SERS enhancement which is consistent with their experimental observations. This suggests that making SERS substrates at lowered temperatures will generate greater enhancements, however, the opposite was found to be true in the study by Oh et al. [43]. In their study, it was found that substrates made at higher temperatures had higher SERS enhancements than substrates made at lower temperature. This was contradictory to what was initially thought, as Ag films made at higher temperatures had lower nanorod densities. This called for a theoretical treatment of their substrate using FDTD. It was found that the greatest SERS EF were contributed to gaps smaller than 3 nm, this led to EFs of up to 10^8 to be derived irrespective of geometrical schemes. Oh et al.'s study also showed that thermal evaporation can make SERS substrates by OAD comparable to those made by e-beam. From these studies, it seems that uncontrolled room temperature oblique angle depositions seem unfavourable for making high performance SERS substrates. There have yet to be temperature-SERS studies done with other substrates, such as polymers, that have significantly different thermal conductivities to typical silicon/glass substrates. While changes in geometries were observed as a temperature dependence during oblique angle depositions, there is little in literature that studies this temperature dependence with other nanostructures [15,53], perhaps this will be a new area that will be expanded in the near future.

3.1.2. Geometries of OAD Derived SERS Substrates

As illustrated before with Figure 8, oblique angle deposition provides a method for making complex and nanostructures simply by manipulating the deposition angle. Substrate rotation during OAD can generate helical structures, Jen et al. have investigated nanohelix arrays using oblique angle

depositions at −140 °C that were applied to SERS investigations. In their 2015 work, they compared nanohelix arrays made from Ag and Au, where it was found that gold was the better SERS material for this configuration [53]. This study compared the SERS spectra of BPE using nanohelix and nanorod arrays made with Ag, Figure 10 is from [53], indicating clearer SERS spectrum with a nanohelix array.

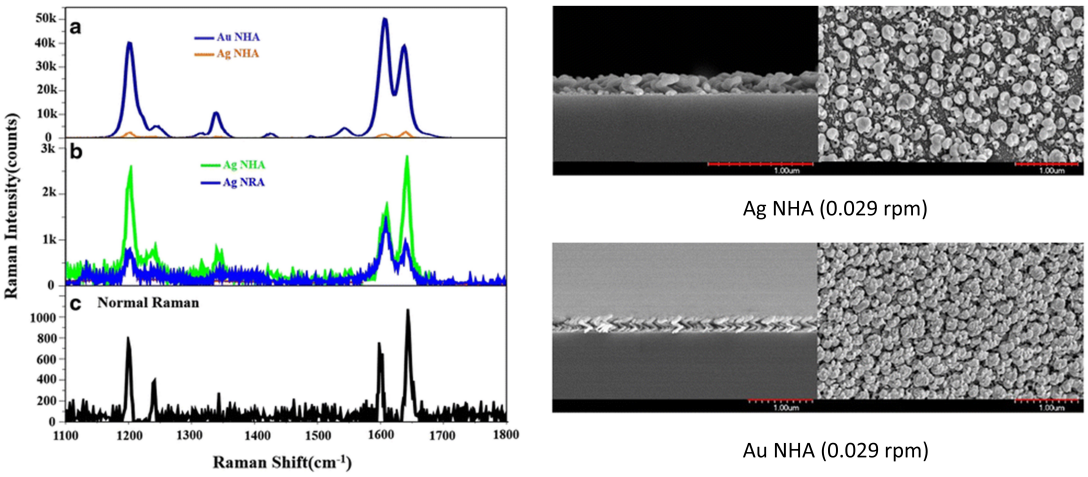

Figure 10. Comparison of BPE SERS spectra on Ag nanohelix and nanorod array, then comparing the Ag nanohelix array with its Au analogue. Reprinted with permission from [53]. Copyright 2015 by Jen et al. based on Creative Commons Attribution 4.0 International License.

From that study, they found that by using a cooled substrate rotation, the film morphology could be controlled as a function of rotation speed. However, it was also material dependent as Ag did not behave like Au under the same deposition conditions. In their more recent 2016 study, the lower the spin rate used, the more hotspots would be supported as the pitch and helical radius increases [15]. Their 3D FDTD simulations of three structures, each based on the resultant nanohelix deposited at their respective rotation speeds, support this as the $|\mathbf{E}/\mathbf{E}_i|$ was found to be greatest for the slowest rotation. Substrate movement isn't just used in OAD for helical structures, it can also be used to generate zigzag-nanorod arrays as done in a study by Keating et al. [17]. These zigzag-nanorod arrays were found to have poorer relative standard deviations in their SERS measurements, 33.4% for zigzag-arrays as opposed to 11.8% for nanorod arrays made at single angles. However, despite this, the zigzag-nanorod array was found (both in DDA simulations and experimental observations) to have greater SERS enhancement than the standard nanorod array. This was attributed to the sharp bends in the zigzag structure allowing the generation of more intense hotspots. OAD is not only used for 2D and 3D structures, but also can be used to make metal films on existing structures. There have been studies into using templates for oblique angle deposition, which will be explored in the next section, in making high quality SERS substrates. One common method of using a template is using the self-assembly nature of polystyrene nanospheres [61,62]. In these cases, the atomic self-shadowing effect is predefined by the nanospheres, so nanoparticles are deposited at regular set intervals. Templates provide an advanced configuration to the OAD technique, where templates can be tailored for individual applications.

3.1.3. Template Assisted Deposition

Templates are surfaces with defined surface structures, so when used in oblique angle depositions, there will be predefined shadowing. This compliments the growth mechanism in oblique angle depositions, where nucleation sites are random and are the start point for the atomic self-shadowing effect [28]. In fact Figure 8 shows nanorods grown on a template, the SEM image showed that

nanorods were positioned in an ABA packing arrangement. Malac et al.'s study, in 1999, was one of the earliest reports using designed nanoscale templates for OAD [63]. Since then, technology has allowed fabrication into smaller dimensions with better control, and now different types of templates exist. Lithography and etching techniques are typically used for making templates [64,65], other methods include self-assembled nanoparticles [61,62] and nano-imprinted polymers [17,18,30]. The advantages of using lithography techniques is that resolutions on the order of 5 nm are achievable, however, the cost and scalability remain a challenge for mass production. Self-assembled polystyrene nanospheres presents a cheaper alternative for OAD templates, however, distribution of nanostructures would be limited to packing arrangements (i.e., hexagonal close packing). Nano-imprinting has been used in SERS substrates for almost a decade [66], but was until recently that researchers had used nano-imprinted polymers as a template for oblique angle deposition derived SERS substrates [30]. To date, literature that refers to the use of OAD templates for SERS applications is limited [17,18,30,65,67–69], even with improved order of nanostructures; SERS reproducibility remains an issue [70]. Theoretical studies have suggested that randomly arranged nanostructures will attain higher enhancements [38], these do acknowledge the fact that suitable SERS substrates require consistency; on its surfaces and batches which are achievable through the use of templates.

3.2. Metal Decorated Nanostructures Made by OAD

SERS materials, typically gold or silver, are expensive. Therefore making nanostructures remain an issue for large area production, as well as the inherent issue of SERS measurement reproducibility between batches. An alternative would be to produce nanostructures using OAD, such as from SiO_2 [71], that would then be deposited with metal nanoparticles for hotspot generation.

Figures from the study by Hou et al. are adapted into Figure 11, by sputtering the nanoparticles onto the nanorod array this metal on oxide SERS substrate is fabricated entirely by PVD processes. An advantage of this is that metal structures can be prone to atmospheric contamination or just oxidation from the air [72], thus by decorating a nanostructure array there would be less wasted SERS-active material. Interestingly, the substrates made by Hou et al. were highly sensitive (with an EF of 10^8) and reusable. There is limited literature in regards to this approach [71], as fabricating these oxide materials can be achieved chemically without the need of a vacuum system. Therefore, there is still more to opportunities for future work in OAD derived SERS substrates.

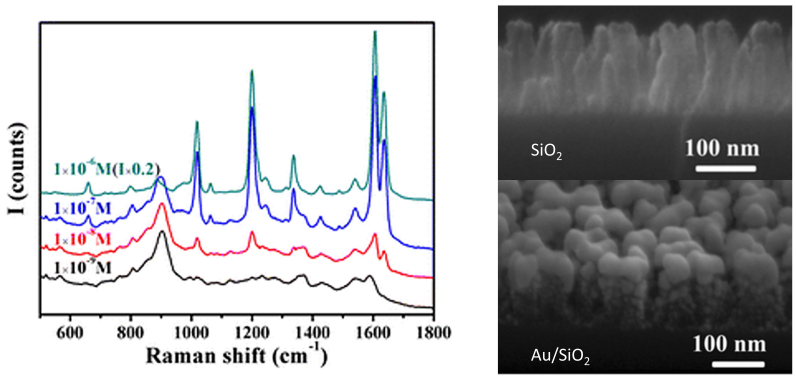

Figure 11. SiO_2 nanorods fabricated by oblique angle deposition at 86° then Au is sputtered onto the nanorod array for 240 s. Reprinted with permission from [71]. Copyright 2015 by Hou et al. based on Creative Commons Attribution 4.0 International License.

4. Application of OAD Derived SERS Substrates

SERS presents a powerful analytical method that requires little sample preparation and possesses up to single-molecule sensitivities. The field is very interdisciplinary, from understanding the

fundamental physical processes behind the enhancements to biomedical applications. Combined with the oblique angle deposition, vast kinds of SERS substrates can be made possible, in this section the applications of such substrates will be explored. Potential uses for OAD derived SERS can be categorised into; biological and biomedical, chemical analysis and security applications.

4.1. Biological and Biomedical Applications

Raman scattering is sensitive to the molecular environment and therefore "fingerprints" of spectra can be used to identify samples. This fingerprinting method is typically used in biological SERS studies to help identify species of bacteria. SERS can also be used to detect by-products from the metabolism of living cells, thereby in-situ monitoring of a biological system is possible. In this section, the applications of OAD derived SERS in bacteria, biomedical and drug studies will be explored.

4.1.1. Bacteria Applications

Rapid identification of pathogens are important for medical strategies. Despite the advances made with SERS sensing of bacteria [73–75] and viruses [76,77], it has yet to be implemented clinically as standard procedure. Traditional techniques such as fluorescence spectroscopy, polymerase chain-reaction (PCR) and cell culture techniques are still the standard methods employed in identification of pathogens. These techniques require specific training, equipment can be expensive and time-consuming. SERS however, requires relatively less intensive training, as sample preparation only require the deposition of cells onto the substrate. Optimised substrates have been reported to produce sensitivities of detecting single *E. coli* bacterium in 10 µL [78]. An issue with using silver nanorods, is that silver can be cytotoxic to bacteria so the binding between surface and sample may not be favoured. One method of resolving this is to functionalise the surface with a material that interacts with both the silver and cell walls of bacteria. Vancomycin (see Figure 12) is one such antibiotic that is used in OAD derived SERS substrates, the mechanism with bacteria is that it forms hydrogen bonds with the peptidoglycan layer which interferes with cell wall synthesis. This is why the antibiotic is not as effective against gram-negative bacteria.

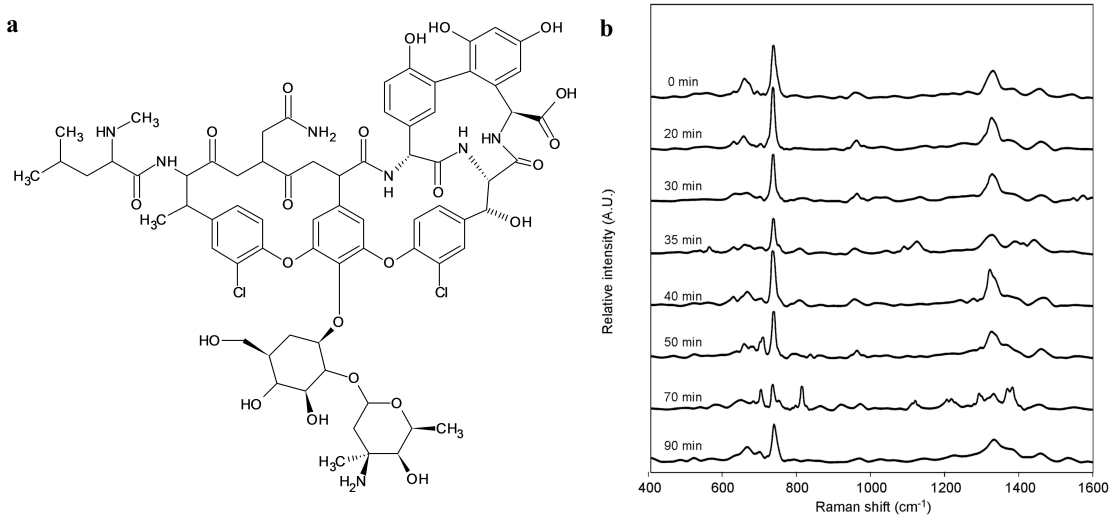

Figure 12. (**a**) Molecular structure of Vancomycin; (**b**) Single bacterium Raman measurement taken, every 10 min for 90 min, shows the effects vancomycin exposure has to *S. aureus*. (**b**) is reprinted with permission from [79]. Copyright 2009 by Liu et al., article under the terms of the Creative Commons Attribution License.

The time elapsed Raman measurements shown in Liu et al.'s study in 2009 [79] shows a measurable change in the SERS spectra for *S. aureus*, as time progresses, the cell wall synthesis being affected by vancomycin becomes that is reflected in the spectra. Whereas in the same time scale, without antibiotics the SERS spectra for *S. aureus* remains consistent. While this proved that SERS has potential for rapid assays (that can take days through conventional methods) the substrate, however, was not made by oblique angle deposition. In a recent study, by Wu et al. [75], vancomycin functionalised SERS substrates were made with nanorod arrays via OAD (that was based on the optimal substrates from their previous study in [73]). With their SERS measurements, they were able to discern serotype information based on the surface proteins with chemometric analysis (see Figure 13). Principal component analysis (PCA) was conducted along with hierarchical cluster analysis (HCA) in order to discern between different species of bacteria. The change in Raman spectra due to the presence of vancomycin is consistent with the earlier study by Liu et al., therefore, not only does SERS presents a rapid method of identifying bacteria (sample exposure time was 5 s in the SERS study [75]) but it also identifies a potential future antibiotic studies. Surface functionalisation has been applied to testing antibiotic susceptibility; from the recent work done by Liu et al. [74], minimum inhibitory concentrations and antibiotic susceptibility tests could be carried out with results that were consistent with incubation methods.

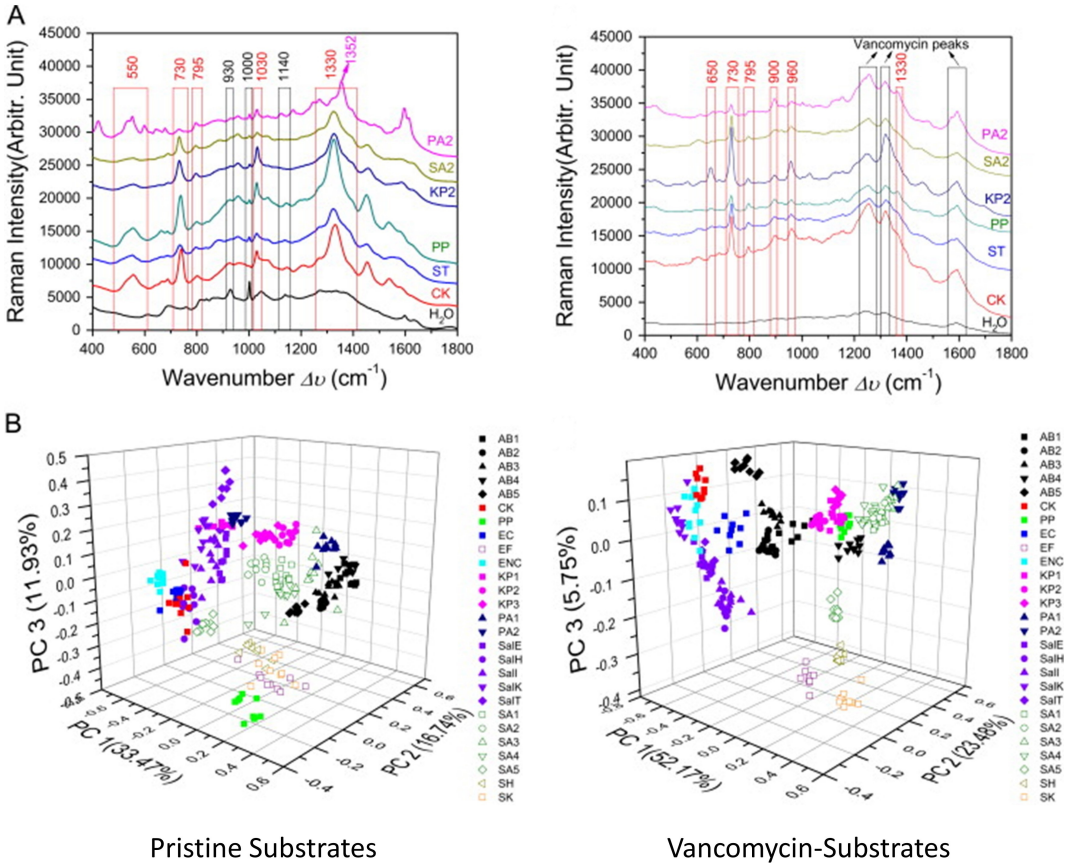

Figure 13. (**A**) SERS spectra for the range of bacteria studied in [75], pristine substrates were harder to differentiate as more environmental contamination (highlighted in the spectra) seem to be present; (**B**) Principal component analysis showed that with the use of vancomycin the correlation between different bacteria was improved. Reprinted with permission from [75]. Copyright 2015 Elsevier.

These types of studies has yet to be done with SERS substrates made with OAD, but other bacteria research has; particularly for biomedical applications.

4.1.2. Biomedical Applications

As discussed in the last section, rapid identification of bacteria is becoming more feasible with SERS, a recent report showed that pathogens from human serum could be identified [80]. Current medical diagnostic methods are more time-consuming, expensive and require more training in order to produce a result. SERS is an attractive tool for diagnostics because of the simpler sample preparation, high sensitivity and speed. One biomedical application is the detection of urea in human serum [81]. Urea levels in the human serum can be used to help diagnose diseases, as well as, characterising kidney function. Identifying the pathogens in patient's blood can be vital, especially when dealing with time-sensitive treatments, SERS can offer rapid bacteria detection in bodily fluids [82,83]. Driskell et al. have made studies into using OAD-based SERS substrates for the detection of rotaviruses [82], group A rotaviruses are known to be infectious and commercially available assays do not provide information on genotypes which are important for disease control and identifying new strains. Typing can be achieved by an Enzyme-linked immunosorbent assay (ELISA) or hemi-nested RT-PCR, however, these techniques are both labour intensive and time-consuming. In [82] the SERS spectra was used in a partial least squares discriminant analysis to classify samples, such that in a cross validation prediction of rotavirus type attained a 100% accuracy. In a recent study by Chen et al., the use of OAD-derived SERS substrates was applied to the detection of early stage malaria [83]. The SERS strategy for detecting malaria revolves around hemozoin, the Raman spectra was taken within its natural environment [84], however early stages of infection contains little hemozoin and maturing parasites lead to mechanisms that make detecting infected red blood cells more difficult to detect. Ag nanorod arrays produced by OAD enable sensitive and reliable detection for infected red blood cells, Figure 14 shows the difference that is seen in the SERS spectra, coupled with PCA (see Figure 15) the study was able to detect different stages of infection.

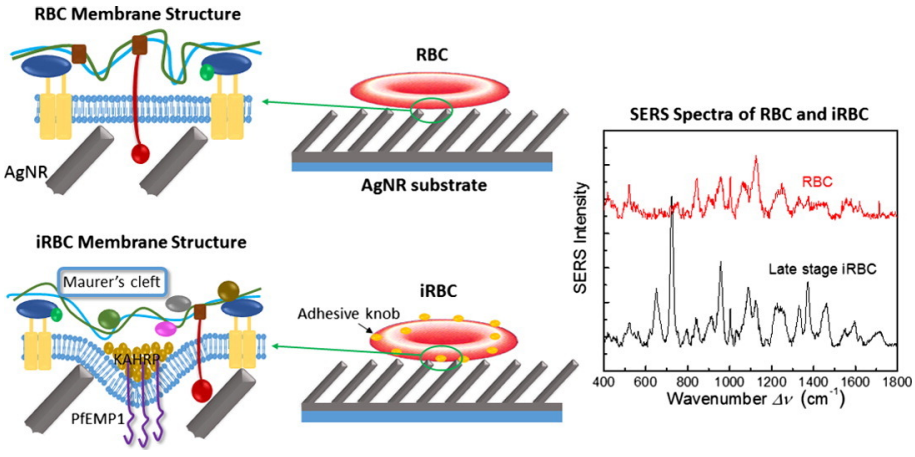

Figure 14. Graphical abstract showing the structural differences in healthy and infected red blood cells, which is also reflected in their SERS spectra. Reprinted with permission from [85]. Copyright 2016 Elsevier.

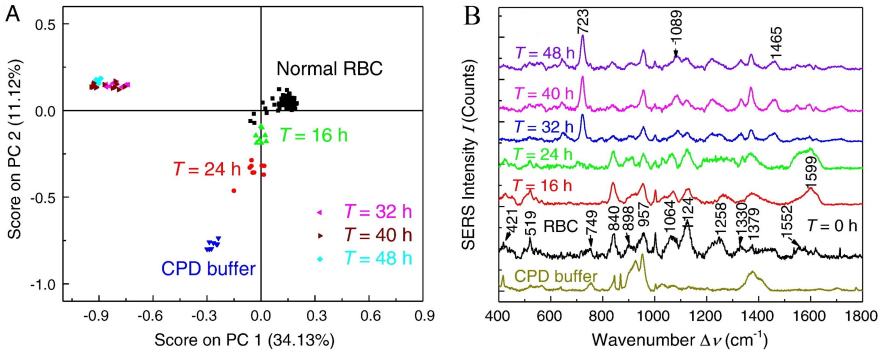

Figure 15. (**a**) PCA based on the SERS spectra of CPD buffer, normal red blood cell and infected cells at different infection times; (**b**) SERS spectra for CPD buffer, normal red blood cell and infected cells at different infection times. Reprinted with permission from [85]. Copyright 2016 Elsevier.

From detecting components in bodily fluids to sensing bacteria, viruses and parasites; SERS proves to be an important diagnostic tool for future clinical use. OAD-derived SERS substrates over the last decade, have been applied to such biosensing applications and continues to contribute new findings.

4.2. Reusable SERS Substrates

SERS substrates can be prone to environmental contamination, over time even noble metals such as Ag react with oxygen that will affect substrate performance. Once used, substrates are difficult to clean without damaging the substrate and/or affecting performance. This small section will discuss how recyclable SERS substrates can be. Ma et al. have used OAD for reusable SERS substrates [86,87], where the metal nanorod arrays are further coated with a transition metal oxide. In [86], TiO_2 was used as a thin protective layer to prevent oxidation and sulfuration of the Ag nanorod array. Here the substrates could be renewed through simple ultraviolet illumination and water dilution. Another approach with TiO_2 is found in [88], where instead oblique angle deposition is used for TiO_2 nanorod arrays that are then decorated with Ag nanoparticles. These substrates also have the ability to regenerate via ultraviolet irradiation and could be used to monitor the photocatalytic decomposition of dyes via their SERS spectra. HfO_2 was shown to also improve stability, because HfO_2 possesses a high melting point, heating cycles could also be applied to the SERS substrate in order to regenerate for further use [87]. These protective layers also enable the repeated use in vapour and liquid phase detection, which would be useful for industrial and security applications.

4.3. Food and Security Applications

Food quality is constantly monitored in the industry to ensure products are safe for human consumption. Public security on the other hand are more concerned with detection of any immediate hazards, such as explosives. SERS is one powerful tool that can be applied for these applications, in food inspections it is important to monitor both biological and chemical components. For security purposes, detecting the lowest concentrations of an explosive and/or its by-products is vital. In this section, applications to agriculture, food-safety and explosives will be discussed.

4.3.1. Agriculture and Food-Safety Applications

SERS substrates made by OAD have been used for food-safety applications [89], the SERS spectra in these instances can be complimentary with ultra-thin layer chromatography. During the chromatography, mixtures are separated into different components, that can be assessed via SERS. This combination of techniques can detect potential adulteration of food products, potentially more sensitive and faster than relying on other analytical chemistry techniques. Another instance where

SERS can be used for food-safety, is in the detection of melamine in animal feed [90]. This SERS study was carried out on melamine, as conventional chemical testing methods are gas-liquid chromatography or high performance liquid chromatography, which are more complicated and require significantly more training. The study also showed improved stability and detection times when using a modified clean up step on these SERS substrates. Bacteria is also an important factor to monitor in food products, SERS is not only limited to biomedical applications when it comes to rapid food borne pathogens. Using vancomycin functionalised Ag nanorod arrays made by OAD, Wu et al. were able to detect *S. poona* and *E. coli* from fresh produce [91]. The limits of detection were improved by using a two-step filtration process, that involved a modified PTFE hydrophobic filter treated with (HeptadecaFluoro-1, 1, 2, 2-tetra-hydrodecyl) trichlorosilane. This resulted in limits of detections of 100 CFU/mL in under 4 h for *S. poona* and *E. coli* at 1000 CFU/mL. This limit of detection for *E. coli* is one of the best reported for label-free SERS and matches with the reported value of [78]. These improvements to the SERS technique and the potential to reuse substrates enable this method to become more portable, which is particularly useful for security purposes.

4.3.2. Explosive Components Detection

SERS is known for its label-free and high sensitivity, that is why this technique is used for the trace-level detection. There has been a lot of research in the area of detecting explosive components/by-products [92,93], however, there is limited literature involving OAD derived SERS in this area [31]. The work done by Nuntawong et al. have shown the use of oblique magnetron sputtering deposition, which in itself is rare. Their SERS substrates claim to have nanorods of 1 micron in length with approximately 100 nm in width, which seems inconsistent with their FE-SEM image's scale bar. Despite this, it is promising to see their measurements can discern the perchlorate peak which is useful for the detection of explosives, as well as, the significant different to the SERS spectra between dissolved explosives and burned explosives. Current developments have yet to yield an OAD derived SERS substrate that can sense in the gas, liquid and solid phases. One method uses Au nanoparticles which is capable of examining analytes both in the liquid and non-liquid phases [94]. Therefore, as most of the research here has had biomedical themes, there presents a great opportunity of future work in the area of OAD-derived SERS in detecting explosives.

5. Conclusions

This review has presented a number of topics, from computational calculations to applications of substrates made by OAD, all in order to better our understanding and use of SERS. Oblique angle deposition is simple technique that yields complex nanostructures, yet there is still more to be understood about deposition processes when it comes to metal depositions. Simple controls such as substrate temperature have allowed us to further manipulate nanostructures with the same deposition technique. Using OAD has enhanced the field of SERS, recent developments have enabled us to potentially detect earlier stages malaria from spectral changes to malarial infected blood cells. While this field has strength in biological applications, there is still potential research to be done in environmental sensing and the underlying physics of the SERS phenomenon. Electrodynamic simulations enable us to understand the mechanisms involved in the phenomenon of surface-enhanced Raman scattering and it is anticipated that future OAD-SERS research will include theoretical treatments to the deposition processes. In conclusion, with Raman equipment becoming more affordable and portable, we expect to see applications of OAD derived SERS in more fields.

Acknowledgments: Thanks go to the Institute of Thin Films, Sensors & Imaging (TFSI) at the School of Engineering and Computing at the University of the West of Scotland, the Scottish Universities Physics Alliance (SUPA).

Conflicts of Interest: The authors declare no conflict of interest.

Abbreviations

The following abbreviations are used in this manuscript:

BPE	1,2-Bis(4-Pyridyl)Ethylene
CV	Crystal Violet
DDA	Discrete Dipole Approximation
DFT	Desity Functional Theory
EF	Enhancement Factor
FDTD	Finite-Difference Time Domain
GLAD	Glancing Angle Deposition
HCA	Hierarchical Cluster Analysis
LSPR	Localised Surface Plasmon Resonance
OAD	Oblique Angle Deposition
PCA	Principal Component Analysis
PCR	Polymerase Chain-Reaction
PECVD	Plasma Enhanced Chemical Vapour Deposition
PVD	Physical Vapour Deposition
SERS	Surface Enhanced Raman Scattering

References

1. Raman, C. A new radiation. *Indian J. Phys.* **1928**, *2*, 387–398.
2. Wang, W. Identification of CVD Synthetic Gem Diamond Using Raman Spectroscopy. In Proceedings of the 11th International GeoRaman Conference, St. Louis, MO, USA, 15–19 June 2014.
3. Fleischmann, M.; Hendra, P.; McQuillan, A. Raman spectra of pyridine adsorbed at a silver electrode. *Chem. Phys. Lett.* **1974**, *26*, 163–166.
4. Lombardi, J.R.; Birke, R.L.; Lu, T.; Xu, J. Charge-transfer theory of surface enhanced Raman spectroscopy: Herzberg–Teller contributions. *J. Chem. Phys.* **1986**, *84*, 4174–4180.
5. Chen, L.; Gao, Y.; Cheng, Y.; Li, H.; Wang, Z.; Li, Z.; Zhang, R.Q. Nonresonant chemical mechanism in surface-enhanced Raman scattering of pyridine on M@Au12 clusters. *Nanoscale* **2016**, *8*, 4086–4093.
6. Kneipp, K.; Kneipp, H.; Manoharan, R.; Hanlon, E.B.; Itzkan, I.; Dasari, R.R.; Feld, M.S. Extremely Large Enhancement Factors in Surface-Enhanced Raman Scattering for Molecules on Colloidal Gold Clusters. *Appl. Spectrosc.* **1998**, *52*, 1493–1497.
7. Jeanmaire, D.L.; Van Duyne, R.P. Surface raman spectroelectrochemistry. *J. Electroanal. Chem. Interfacial Electrochem.* **1977**, *84*, 1–20.
8. Kneipp, K.; Wang, Y.; Kneipp, H.; Perelman, L.T.; Itzkan, I.; Dasari, R.R.; Feld, M.S. Single Molecule Detection Using Surface-Enhanced Raman Scattering (SERS). *Phys. Rev. Lett.* **1997**, *78*, 1667–1670.
9. Le Ru, E.C.; Blackie, E.; Meyer, M.; Etchegoin, P.G. Surface Enhanced Raman Scattering Enhancement Factors: A Comprehensive Study. *J. Phys. Chem. C* **2007**, *111*, 13794–13803.
10. Cao, J.; Sun, T.; Grattan, K.T. Gold nanorod-based localized surface plasmon resonance biosensors: A review. *Sens. Actuators B: Chem.* **2014**, *195*, 332–351.
11. Willets, K.A.; Van Duyne, R.P. Localized surface plasmon resonance spectroscopy and sensing. *Annu. Rev. Phys. Chem.* **2007**, *58*, 267–297.
12. Botta, R.; Rajanikanth, A.; Bansal, C. Silver nanocluster films for glucose sensing by Surface Enhanced Raman Scattering (SERS). *Sens. Bio-Sens. Res.* **2016**, *9*, 13–16.
13. Vinod, M.; Gopchandran, K. Bimetallic Au-Ag nanochains as SERS substrates. *Curr. Appl. Phys.* **2015**, *15*, 857–863.
14. Radziuk, D.; Moehwald, H. Prospects for plasmonic hot spots in single molecule SERS towards the chemical imaging of live cells. *Phys. Chem. Chem. Phys.* **2015**, *17*, 21072–21093.
15. Jen, Y.J.; Huang, J.W.; Liu, W.C.; Chan, S.; Tseng, C.H. Glancing angle deposited gold nanohelix arrays on smooth glass as three-dimensional SERS substrates. *Opt. Mater. Express* **2016**, *6*, 697–704.
16. Driskell, J.D.; Shanmukh, S.; Liu, Y.; Chaney, S.B.; Tang, X.J.; Zhao, Y.P.; Dluhy, R.A. The Use of Aligned Silver Nanorod Arrays Prepared by Oblique Angle Deposition as Surface Enhanced Raman Scattering Substrates. *J. Phys. Chem. C* **2008**, *112*, 895–901.

17. Keating, M.; Song, S.; Wei, G.; Graham, D.; Chen, Y.; Placido, F. Ordered Silver and Copper Nanorod Arrays for Enhanced Raman Scattering Created via Guided Oblique Angle Deposition on Polymer. *J. Phys. Chem. C* **2014**, *118*, 4878–4884.
18. Chu, H.; Song, S.; Gibson, D.; Porteous, L. Glancing angle deposition of silver nanostructures for use in surface enhanced Raman scattering. In Proceedings of the SPIE 9627, Advances in Optical Thin Films V, Jena, Germany, 7–10 September 2015; doi:10.1117/12.2191297.
19. Wu, W.; Hu, M.; Ou, F.S.; Li, Z.; Williams, R.S. Cones fabricated by 3D nanoimprint lithography for highly sensitive surface enhanced Raman spectroscopy. *Nanotechnology* **2010**, *21*, 255502.
20. Robbie, K.; Brett, M.J. Sculptured thin films and glancing angle deposition: Growth mechanics and applications. *J. Vac. Sci. Technol. A* **1997**, *15*, 1460–1465.
21. Robbie, K.; Sit, J.C.; Brett, M.J. Advanced techniques for glancing angle deposition. *J. Vac. Sci. Technol. B* **1998**, *16*, 1115–1122.
22. Abelmann, L.; Lodder, C. Oblique evaporation and surface diffusion. *Thin Solid Films* **1997**, *305*, 1–21.
23. Kennedy, S.R.; Brett, M.J.; Toader, O.; John, S. Fabrication of Tetragonal Square Spiral Photonic Crystals. *Nano Lett.* **2002**, *2*, 59–62.
24. Robbie, K.; Beydaghyan, G.; Brown, T.; Dean, C.; Adams, J.; Buzea, C. Ultrahigh vacuum glancing angle deposition system for thin films with controlled three-dimensional nanoscale structure. *Rev. Sci. Instrum.* **2004**, *75*, 1089–1097.
25. He, Y.; Zhao, Y. Advanced multi-component nanostructures designed by dynamic shadowing growth. *Nanoscale* **2011**, *3*, 2361–2375.
26. Barranco, A.; Borras, A.; Gonzalez-Elipe, A.R.; Palmero, A. Perspectives on oblique angle deposition of thin films: From fundamentals to devices. *Prog. Mater. Sci.* **2016**, *76*, 59–153.
27. Ruffino, F.; Torrisi, V.; Marletta, G.; Grimaldi, M.G. Kinetic growth mechanisms of sputter-deposited Au films on mica: From nanoclusters to nanostructured microclusters. *Appl. Phys. A* **2010**, *100*, 7–13.
28. Zhao, Y.; Ye, D.; Wang, G.C.; Lu, T.M. Designing nanostructures by glancing angle deposition. In Proceedings of the SPIE 5219, Nanotubes and Nanowires, San Diego, CA, USA, 3–4 August 2003; doi:10.1117/12.505253.
29. Tait, R.N.; Smyb, T.; Bretta, M.J.; Smy, T.; Brett, M. Modelling and characterization of columnar growth in evaporated films. *Thin Solid Films* **1993**, *226*, 196–201.
30. Song, S.; Keating, M.; Chen, Y.; Placido, F. Reflectance and surface enhanced Raman scattering (SERS) of sculptured silver films deposited at various vapor incident angles. *Meas. Sci. Technol.* **2012**, *23*, 084007.
31. Nuntawong, N.; Eiamchai, P.; Limwichean, S.; Wong-ek, B.; Horprathum, M.; Patthanasettakul, V.; Leelapojanaporn, A.; Nakngoenthong, S.; Chindaudom, P. Trace detection of perchlorate in industrial-grade emulsion explosive with portable surface-enhanced Raman spectroscopy. *Forensic Sci. Int.* **2013**, *233*, 174–178.
32. Rodrigues, D.C.; de Souza, M.L.; Souza, K.S.; dos Santos, D.P.; Andrade, G.F.S.; Temperini, M.L.A. Critical assessment of enhancement factor measurements in surface-enhanced Raman scattering on different substrates. *Phys. Chem. Chem. Phys.* **2015**, *17*, 21294–21301.
33. Hakonen, A.; Svedendahl, M.; Ogier, R.; Yang, Z.J.; Lodewijks, K.; Verre, R.; Shegai, T.; Andersson, P.O.; Kall, M. Dimer-on-mirror SERS substrates with attogram sensitivity fabricated by colloidal lithography. *Nanoscale* **2015**, *7*, 9405–9410.
34. Kanipe, K.N.; Chidester, P.P.F.; Stucky, G.D.; Moskovits, M. Large Format Surface-Enhanced Raman Spectroscopy Substrate Optimized for Enhancement and Uniformity. *ACS Nano* **2016**, *10*, 7566–7571.
35. Hankus, M.E.; Stratis-Cullum, D.N.; Pellegrino, P.M. Surface enhanced Raman scattering (SERS)-based next generation commercially available substrate: Physical characterization and biological application. In Proceedings of the SPIE 8099, Biosensing and Nanomedicine IV, San Diego, CA, USA, 21–23 August 2011; doi:10.1117/12.893842.
36. Lyvers, D.P.; Moon, J.M.; Kildishev, A.V.; Shalaev, V.M.; Wei, A. Gold Nanorod Arrays as Plasmonic Cavity Resonators. *ACS Nano* **2008**, *2*, 2569–2576.
37. Yang, Y.; Hu, Z.; Wang, Y.; Wang, B.; Zhan, Q.; Zhang, Y.; Ao, X. Broadband SERS substrates by oblique angle deposition method. *Opt. Mater. Express* **2016**, *6*, 2644–2654.
38. Wei, G.; Wang, J.; Chen, Y. Electromagnetic enhancement of ordered silver nanorod arrays evaluated by discrete dipole approximation. *Beilstein J. Nanotechnol.* **2015**, *6*, 686–696.
39. Jackson, J.D. *Classical Electrodynamics*; Wiley: New York, NY, USA, 1999; p. 808.

40. Oskooi, A.F.; Roundy, D.; Ibanescu, M.; Bermel, P.; Joannopoulos, J.; Johnson, S.G. MEEP: A flexible free-software package for electromagnetic simulations by the FDTD method. *Comput. Phys. Commun.* **2010**, *181*, 687–702.
41. Yee, K. Numerical solution of initial boundary value problems involving maxwell's equations in isotropic media. *IEEE Trans. Antennas Propag.* **1966**, *14*, 302–307.
42. Parsons, J.; Burrows, C.; Sambles, J.; Barnes, W. A comparison of techniques used to simulate the scattering of electromagnetic radiation by metallic nanostructures. *J. Modern Opt.* **2010**, *57*, 356–365.
43. Oh, M.-K.; Shin, Y.S.; Lee, C.L.; De, R.; Kang, H.; Yu, N.E.; Kim, B.H.; Kim, J.H.; Yang, J.K. Morphological and SERS Properties of Silver Nanorod Array Films Fabricated by Oblique Thermal Evaporation at Various Substrate Temperatures. *Nanoscale Res. Lett.* **2015**, *10*, doi:10.1186/s11671-015-0962-8.
44. Liu, Y.J.; Zhang, Z.Y.; Zhao, Q.; Dluhy, R.A.; Zhao, Y.P. Surface Enhanced Raman Scattering from an Ag Nanorod Array Substrate: The Site Dependent Enhancement and Layer Absorbance Effect. *J. Phys. Chem. C* **2009**, *113*, 9664–9669.
45. Jayawardhana, S.; Rosa, L.; Buividas, R.; Stoddart, P.R.; Juodkazis, S. Light enhancement in surface-enhanced Raman scattering at oblique incidence. *Photon. Sens.* **2012**, *2*, 283–288.
46. Yurkin, M.A.; Hoekstra, A.G.; Brock, R.S.; Lu, J.Q. Systematic comparison of the discrete dipole approximation and the finite difference time domain method for large dielectric scatterers. *Opt. Express* **2007**, *15*, 17902–17911.
47. Draine, B.T.; Flatau, P.J. User Guide for the Discrete Dipole Approximation Code DDSCAT 7.0. **2008**, arXiv:0809.0337.
48. Liu, Y.J.; Zhao, Y.P. Simple model for surface-enhanced Raman scattering from tilted silver nanorod array substrates. *Phys. Rev. B* **2008**, *78*, 075436.
49. Kaempf, F. Größe und Ursache der Doppelbrechung in Kundtschen Spiegeln und Erzeugung von Doppelbrechung in Metallspiegeln durch Zug. *Annal. Phys.* **1905**, *321*, 308–333.
50. Zhang, N.; Su, X.; Free, P.; Zhou, X.; Neoh, K.G.; Teng, J.; Knoll, W. Plasmonic metal nanostructure array by glancing angle deposition for biosensing application. *Sens. Actuators B: Chem.* **2013**, *183*, 310–318.
51. Xi, J.Q.; Schubert, M.F.; Kim, J.K.; Schubert, E.F.; Chen, M.; Lin, S.Y.; Liu, W.; Smart, J.A. Optical thin-film materials with low refractive index for broadband elimination of Fresnel reflection. *Nat. Photon.* **2007**, *1*, 176–179.
52. Zhu, Y.; Jiao, H. Rugate filter with multi-channel grown by glancing angle deposition. *Opt.-Int. J. Light Electron Opt.* **2012**, *123*, 1501–1503.
53. Jen, Y.J.; Chan, S.; Huang, J.W.; Jheng, C.Y.; Liu, W.C. Self-Shadowing Deposited Pure Metal Nanohelix Arrays and SERS Application. *Nanoscale Res. Lett.* **2015**, *10*, doi:10.1186/s11671-015-1205-8.
54. Ruffino, F.; Grimaldi, M.G. Control of the Kinetic Roughening in Nanostructured Ag Films by Oblique Sputter-Depositions. *Nanosci. Nanotechnol. Lett.* **2013**, *4*, 309–315.
55. Dirks, A.; Leamy, H. Columnar microstructure in vapor-deposited thin films. *Thin Solid Films* **1977**, *47*, 219–233.
56. Zhao, Y.P.; Chaney, S.B.; Zhang, Z.Y. Absorbance spectra of aligned Ag nanorod arrays prepared by oblique angle deposition. *J. Appl. Phys.* **2006**, *100*, 063527.
57. Lau, W.F.; Bai, F.; Huang, Z. Ballistic glancing angle deposition of inclined Ag nanorods limited by adatom diffusion. *Nanotechnology* **2013**, *24*, 465707.
58. Lichter, S.; Chen, J. Model for Columnar Microstructure of Thin Solid Films. *Phys. Rev. Lett.* **1986**, *56*, 1396–1399.
59. Singh, J.P.; Lanier, T.E.; Zhu, H.; Dennis, W.M.; Tripp, R.A.; Zhao, Y. Highly Sensitive and Transparent Surface Enhanced Raman Scattering Substrates Made by Active Coldly Condensed Ag Nanorod Arrays. *J. Phys. Chem. C* **2012**, *116*, 20550–20557.
60. Khare, C.; Patzig, C.; Gerlach, J.W.; Rauschenbach, B.; Fuhrmann, B. Influence of substrate temperature on glancing angle deposited Ag nanorods. *J. Vac. Sci. Technol. A* **2010**, *28*, 1002–1009.
61. Ingram, W.M.; Han, C.; Zhang, Q.; Zhao, Y. Optimization of Ag-Coated Polystyrene Nanosphere Substrates for Quantitative Surface-Enhanced Raman Spectroscopy Analysis. *J. Phys. Chem. C* **2015**, *119*, 27639–27648.
62. Giordano, M.C.; Foti, A.; Messina, E.; Gucciardi, P.G.; Comoretto, D.; Buatier de Mongeot, F. SERS Amplification from Self-Organized Arrays of Plasmonic Nanocrescents. *ACS Appl. Mater. Interfaces* **2016**, *8*, 6629–6638.

63. Malac, M.; Egerton, R.F.; Brett, M.J.; Dick, B. Fabrication of submicrometer regular arrays of pillars and helices. *J. Vac. Sci. Technol. B* **1999**, *17*, 2671–2674.
64. He, Z.; Kretzschmar, I. Template-Assisted GLAD: Approach to Single and Multipatch Patchy Particles with Controlled Patch Shape. *Langmuir* **2013**, *29*, 15755–15761.
65. Fu, J.; Cao, Z.; Yobas, L. Localized oblique-angle deposition: Ag nanorods on microstructured surfaces and their SERS characteristics. *Nanotechnology* **2011**, *22*, 505302.
66. Alvarez-Puebla, R.; Cui, B.; Bravo-Vasquez, J.P.; Veres, T.; Fenniri, H. Nanoimprinted SERS-Active Substrates with Tunable Surface Plasmon Resonances. *J. Phys. Chem. C* **2007**, *111*, 6720–6723.
67. Liu, S.S.; Xu, Z.M.; Sun, T.Y.; Zhao, W.N.; Wu, X.H.; Ma, Z.C.; Zhang, X.M.; He, J.; Chen, C.H. SERS-Active Ag Decorated Polymer Nanorod Substrate Fabricated by the Combination of Photochemical Reduction and Nanoimprint Technology. *Adv. Mater. Res.* **2014**, *886*, 101–104.
68. Boltasseva, A. Plasmonic components fabrication via nanoimprint. *J. Opt. A: Pure Appl. Opt.* **2009**, *11*, 114001.
69. Guo, Z.; Chen, L.; Lv, H.; Yu, Z.; Zhao, B. Magnetic imprinted surface enhanced Raman scattering (MI-SERS) based ultrasensitive detection of ciprofloxacin from a mixed sample. *Anal. Methods* **2014**, *6*, 1627–1632.
70. Stoddart, P.R.; Jayawardhana, S. Nanofabrication of surface-enhanced Raman scattering substrates for optical fiber sensors. In Proceedings of the SPIE 8613, Advanced Fabrication Technologies for Micro/Nano Optics and Photonics VI, San Francisco, CA, USA, 5–6 February 2013; doi:10.1117/12.2004019.
71. Hou, M.; Huang, Y.; Ma, L.; Zhang, Z. Sensitivity and Reusability of SiO_2 NRs@ Au NPs SERS Substrate in Trace Monochlorobiphenyl Detection. *Nanoscale Res. Lett.* **2015**, *10*, doi:10.1186/s11671-015-1147-1.
72. Im, H.; Lindquist, N.C.; Lesuffleur, A.; Oh, S.H. Atomic Layer Deposition of Dielectric Overlayers for Enhancing the Optical Properties and Chemical Stability of Plasmonic Nanoholes. *ACS Nano* **2010**, *4*, 947–954.
73. Wu, X.; Xu, C.; Tripp, R.A.; Huang, Y.w.; Zhao, Y. Detection and differentiation of foodborne pathogenic bacteria in mung bean sprouts using field deployable label-free SERS devices. *Analyst* **2013**, *138*, 3005–3012.
74. Liu, C.Y.; Han, Y.Y.; Shih, P.H.; Lian, W.-N.; Wang, H.-H.; Lin, C.-H.; Hsueh, P.-R.; Wang, J.-K.; Wang, Y.-L. Rapid bacterial antibiotic susceptibility test based on simple surface-enhanced Raman spectroscopic biomarkers. *Sci. Rep.* **2016**, *6*, 23375.
75. Wu, X.; Huang, Y.W.; Park, B.; Tripp, R.A.; Zhao, Y. Differentiation and classification of bacteria using vancomycin functionalized silver nanorods array based surface-enhanced Raman spectroscopy and chemometric analysis. *Talanta* **2015**, *139*, 96–103.
76. Tripp, R.A.; Dluhy, R.A.; Zhao, Y. Novel nanostructures for SERS biosensing. *Nano Today* **2008**, *3*, 31–37.
77. Negri, P.; Choi, J.Y.; Jones, C.; Tompkins, S.M.; Tripp, R.A.; Dluhy, R.A. Identification of virulence determinants in influenza viruses. *Anal. Chem.* **2014**, *86*, 6911–6917.
78. Srivastava, S.K.; Hamo, H.B.; Kushmaro, A.; Marks, R.S.; Grüner, C.; Rauschenbach, B.; Abdulhalim, I. Highly sensitive and specific detection of *E. coli* by a SERS nanobiosensor chip utilizing metallic nanosculptured thin films. *Analyst* **2015**, *140*, 3201–3209.
79. Liu, T.T.; Lin, Y.H.; Hung, C.S.; Liu, T.J.; Chen, Y.; Huang, Y.C.; Tsai, T.H.; Wang, H.H.; Wang, D.W.; Wang, J.K.; et al. A High Speed Detection Platform Based on Surface-Enhanced Raman Scattering for Monitoring Antibiotic-Induced Chemical Changes in Bacteria Cell Wall. *PLoS ONE* **2009**, *4*, 1–10.
80. Kotanen, C.N.; Martinez, L.; Alvarez, R.; Simecek, J.W. Surface enhanced Raman scattering spectroscopy for detection and identification of microbial pathogens isolated from human serum. *Sens. Bio-Sens. Res.* **2016**, *8*, 20–26.
81. Han, Y.A.; Ju, J.; Yoon, Y.; Kim, S.M. Fabrication of cost-effective surface enhanced Raman spectroscopy substrate using glancing angle deposition for the detection of urea in body fluid. *J. Nanosci. Nanotechnol.* **2014**, *14*, 3797–3799.
82. Driskell, J.D.; Zhu, Y.; Kirkwood, C.D.; Zhao, Y.; Dluhy, R.A.; Tripp, R.A. Rapid and Sensitive Detection of Rotavirus Molecular Signatures Using Surface Enhanced Raman Spectroscopy. *PloS ONE* **2010**, *5*, 1–9.
83. Chen, F.; Flaherty, B.R.; Cohen, C.E.; Peterson, D.S.; Zhao, Y. Direct detection of malaria infected red blood cells by surface enhanced Raman spectroscopy. *Nanomed. Nanotechnol. Biol. Med.* **2016**, *12*, 1445–1451.
84. Wood, B.R.; Langford, S.J.; Cooke, B.M.; Glenister, F.K.; Lim, J.; McNaughton, D. Raman imaging of hemozoin within the food vacuole of Plasmodium falciparum trophozoites. *FEBS Lett.* **2003**, *554*, 247–252.
85. Chen, K.; Zhang, X.; Zhang, Y.; Lei, D.Y.; Li, H.; Williams, T.; MacFarlane, D.R. Highly Ordered Ag/Cu Hybrid Nanostructure Arrays for Ultrasensitive Surface-Enhanced Raman Spectroscopy. *Adv. Mater. Interfaces* **2016**, *3*, 1600115.

86. Ma, L.; Huang, Y.; Hou, M.; Xie, Z.; Zhang, Z. Ag Nanorods Coated with Ultrathin TiO_2 Shells as Stable and Recyclable SERS Substrates. *Sci. Rep.* **2015**, *5*, doi:10.1038/srep15442.
87. Ma, L.; Wu, H.; Huang, Y.; Zou, S.; Li, J.; Zhang, Z. High-Performance Real-Time SERS Detection with Recyclable Ag Nanorods@HfO2 Substrates. *ACS Appl. Mater. Interfaces* **2016**, *8*, 27162–27168.
88. Kumar, S.; Lodhi, D.K.; Singh, J.P. Highly sensitive multifunctional recyclable Ag-TiO_2 nanorod SERS substrates for photocatalytic degradation and detection of dye molecules. *RSC Adv.* **2016**, *6*, 45120–45126.
89. Wu, X.; Chen, J.; Park, B.; Huang, Y.W.; Zhao, Y. The Use of Silver Nanorod Array-Based Surface-Enhanced Raman Scattering Sensor for Food Safety Applications. In *Advances in Applied Nanotechnology for Agriculture*; American Chemical Society: Washington, DC, USA, 2013; pp. 85–108.
90. Cheng, J.; Su, X.O.; Yao, Y.; Han, C.; Wang, S.; Zhao, Y. Highly Sensitive Detection of Melamine Using a One-Step Sample Treatment Combined with a Portable Ag Nanostructure Array SERS Sensor. *PLoS ONE* **2016**, *11*, doi:10.1371/journal.pone.0154402 .
91. Wu, X.; Han, C.; Chen, J.; Huang, Y.W.; Zhao, Y. Rapid Detection of Pathogenic Bacteria from Fresh Produce by Filtration and Surface-Enhanced Raman Spectroscopy. *JOM* **2016**, *68*, 1156–1162.
92. Hakonen, A.; Andersson, P.O.; Stenbæk Schmidt, M.; Rindzevicius, T.; Käll, M. Explosive and chemical threat detection by surface-enhanced Raman scattering: A review. *Anal. Chim. Acta* **2015**, *893*, 1–13.
93. Zapata, F.; López-López, M.; García-Ruiz, C. Detection and identification of explosives by surface enhanced Raman scattering. *Appl. Spectrosc. Rev.* **2016**, *51*, 227–262.
94. Yang, S.; Dai, X.; Stogin, B.B.; Wong, T.S. Ultrasensitive surface-enhanced Raman scattering detection in common fluids. *Proc. Natl. Acad. Sci. USA* **2016**, *113*, 268–273.